Swen Grossmann*, Rosa Maria Staufer, Niels Grabow, Valeria Khaimov, Klaus-Peter Schmitz, and Stefan Siewert

Laser-induced periodic surface structures for controlled cell growth on vascular stents

https://doi.org/10.1515/cdbme-2025-0114

Abstract: Stents play a vital role in the treatment of cardiovascular diseases. In this context, endothelialization is of crucial importance for the final implant performance and the key to an effective treatment. To enhance endothelial cell (EC) attachment and surface coverage, laser-induced periodic surface structures (LIPSS) have been identified as an effective surface modification technique. This study examines the effects of groove-like and spike-like LIPSS on EC behavior using femtosecond laser-machined stainless steel substrates. The fabricated structures were evaluated with respect to EC orientation and morphology through *in vitro* experiments. The findings indicate that groove-like LIPSS notably impact EC orientation, demonstrating their ability to enhance endothelialization. Additionally, a stainless steel stent featuring groove-like LIPSS was produced, illustrating the feasibility of incorporating LIPSS into industrial fabrication processes for cardiovascular implants. This study underscores the potential of LIPSS to enhance stent biocompatibility and long-term performance.

Keywords: Femtosecond laser ablation, Laser-induced periodic surface structures, LIPSS, implants, stents

1 Introduction

Cardiovascular diseases remain a leading cause of mortality worldwide. In this context, stents play a crucial role in the treatment of arteriosclerosis, arterial dissections, and aneurysms. Despite their widespread use, stents still come along with complications such as in-stent restenosis and thrombosis, which are primarily influenced by inadequate endothelialization. To address these challenges, surface modifications of stents have been proposed to enhance EC adhesion and proliferation [1, 2].

***Corresponding author: Swen Grossmann,** Institute for ImplantTechnology and Biomaterials e.V., Friedrich-Barnewitz-Str.4, 18119 Rostock-Warnemünde, Germany, e-mail: swen.grossmann@iib-ev.de
Rosa Maria Staufer, Valeria Khaimov, Klaus-Peter Schmitz, Stefan Siewert, Institute for ImplantTechnology and Biomaterials e.V., 18119 Rostock-Warnemünde, Germany
Niels Grabow, Institute for Biomedical Engineering, Rostock University Medical Center, 18119 Rostock-Warnemünde, Germany

One promising concept is the structuring of stent surfaces using LIPSS, periodic structures on the nanometer or micrometer scale generated by direct laser irradiation [3, 4]. LIPSS can manifest as grooves, spikes, or more complex shapes. Especially nano-scaled highly periodic LIPSS, such as grooves, have been shown to effectively modulate cellular orientation, elongation, and density, particularly for smooth muscle and ECs [5]. However, the use of LIPSS on commercial implants is limited by the implementation of fabrication processes into existing industrial systems.

Within this study, we investigate the use of LIPSS for controlling the EC behavior on stainless steel with respect to application on metal stents. We first evaluate the functionality of the LIPSS by analyzing the proliferation and morphology of ECs. For this purpose, two types of LIPSS, groove-like and spike-like, are fabricated on stainless steel plates. Subsequently, *in vitro* experiments were performed to characterize the cell-biomaterial interactions. It is shown that the surface structure influences cell orientation. Finally, a stainless steel stent featuring groove-like LIPSS was fabricated, demonstrating the feasibility and simplicity of integrating surface structuring into industrial manufacturing processes of cardiovascular implants.

2 Methods

2.1 Femtosecond laser machining

In order to structure substrates for cell culture experiments, stainless steel plates (316L, 24 mm x 24 mm x 0.5 mm) were first mirror-polished and cut into disks (6 mm diameter) by using a femtosecond laser system embedded into a commercial 4-axis CNC system (Monaco 1035-80-60, Coherent Inc., USA and StarCut Tube Monaco, Coherent Munich GmbH & Co. KG, Germany). A laser pulse duration of 300 fs, a pulse repetition rate of 500 kHz, and a pulse energy of 50 µJ were used. The beam diameter is about 22 µm in the focal plane according to the knife edge method. In a second step, the polished disks were positioned in the laser system, and subsequently, 50% of each disk was structured by scanning the surface with the laser beam as illustrated in Figure 1. The laser beam was linearly polarized along the y-direction and thus perpendicular

to the scan-direction to fabricate highly oriented groove-like LIPSS. The fabrication of spike-like LIPSS had to be done by circular polarization of the laser beam. For both types of nanostructures, the repetition rate and the pulse energy were set to 1 kHz and 4.3 µJ, respectively, while the traverse speed was kept at 5 mm·s^{-1}. In order to obtain very homogeneous LIPSS throughout the scanned area, a line separation in the y-direction of 5 µm was used. The structured metal plates were sonicated for 10 min in ethanol and distilled water.

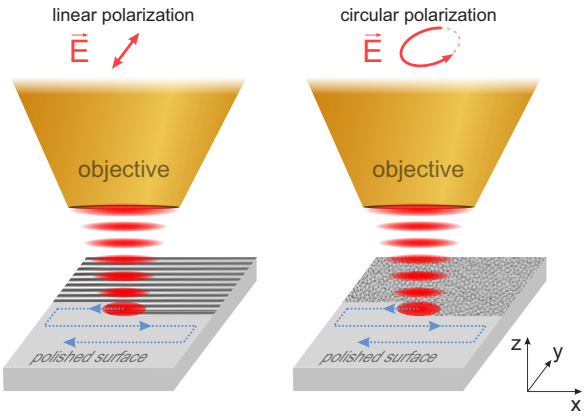

Fig. 1: Illustration of the laser-induced periodic surface structure (LIPSS) fabrication process. The mirror-polished steel surface is scanned line by line with an interline distance of 5 µm. Groove-like LIPSS were fabricated using linear polarization of the laser beam and spike-like LIPSS by circular polarization.

To implement the LIPSS on a stent, an electro-polished stainless steel stent was mounted on an aluminum oxide mandrel, fitting the inner diameter of the stent. The mandrel enables precise positioning of the stent in the laser system, preventing inertia-induced movements of the stent during structuring. For LIPSS fabrication on the stent surface, the same process parameters were applied as for the metal plates.

For analyzing the LIPSS, the metal substrates as well as the structured stent were imaged by means of scanning electron microscopy (Quattro S, Thermo Fisher Scientific Inc., USA). The electron micrographs were obtained using an acceleration voltage of 15 kV and a secondary electron detector. Atomic-force microscopy (AFM) (Nanowizard, JPK Instruments AG, Germany, now Bruker) was used for 3D-imaging of the structured and non-structured surfaces.

2.2 Cell culture

EA.hy 926 (ATCC CRL-2922), an endothelial cell line, was cultured in DMEM supplemented with 10% fetal bovine serum (FBS) and 1% penicillin/streptomycin. Cells were incubated at 37 °C, 5% CO_2, and 78% relative humidity. Next, structured metal plates were placed into 96-well microtiter plates, sterilized with 70% ethanol (non-denatured) for 10 min, and rinsed three times with sterile water. After trypsinization, 5000 cells per well were seeded onto the plates and incubated for 48 h at 37 °C. Finally, the cells were washed with PBS, fixed with 4% formaldehyde for 20 min, and permeabilized with 0.2% Triton X-100. Cytoskeletal staining was performed using either Phalloidin DY-488 or ActinRed^{TM} 555 ReadyProbes^{TM} reagent, with an incubation time of 1 h at room temperature. Nuclear staining with Hoechst 33342 was performed for 10 min. The cells were washed three times with PBS between each step and after staining.

2.3 Cell analysis

Fluorescent imaging was performed using an upright microscope (BX53M, Olympus, Japan). Images were acquired with a 10x-objective (LMPlanFL N 10x, Olympus, Japan) and subsequently processed by ImageJ or Python to optimize brightness and contrast for cell segmentation. The cell segmentation was performed using Cellpose, a gradient-based segmentation tool [6]. Here, a neural network predicts the gradient field within the image, followed by a gradient tracking analysis to identify individual cells. All images were segmented with the pre-trained model cyto3 [7]. Further statistical analysis of cell orientation and cell aspect ratio was performed with Python.

3 Results and discussion

First, the stainless steel substrates were structured using a femtosecond laser system. Two distinct types of structures were fabricated: groove-like and spike-like LIPSS. AFM was employed to obtain a three-dimensional characterization of the surface morphology. Figure 2a shows an AFM map and one extracted height profile of the groove-like LIPSS. The 2D Fast Fourier Transformation (FFT) of the AFM map reveals a structure periodicity of 940 nm, which is very homogeneous throughout the structured area. In contrast to ripple-like LIPSS, the grooves are strictly directed. The root mean square (RMS) of the AFM map is 74 nm. The height profile was used to calculate the mean value of the peak-to-valley height difference of 181 nm $\pm$ 21 nm.

The second type of LIPSS is illustrated in Figure 2b. This spike-like structure shows no preferential direction. As expected, the corresponding FFT is radially symmetric, reflecting a structure periodicity of 948 nm $\pm$ 4 nm, measured in four

directions. The RMS of the structure is 73 nm, which is similar to the groove-like LIPSS. The peak-to-valley height difference extracted from the shown profile is 102 nm $\pm$ 62 nm.

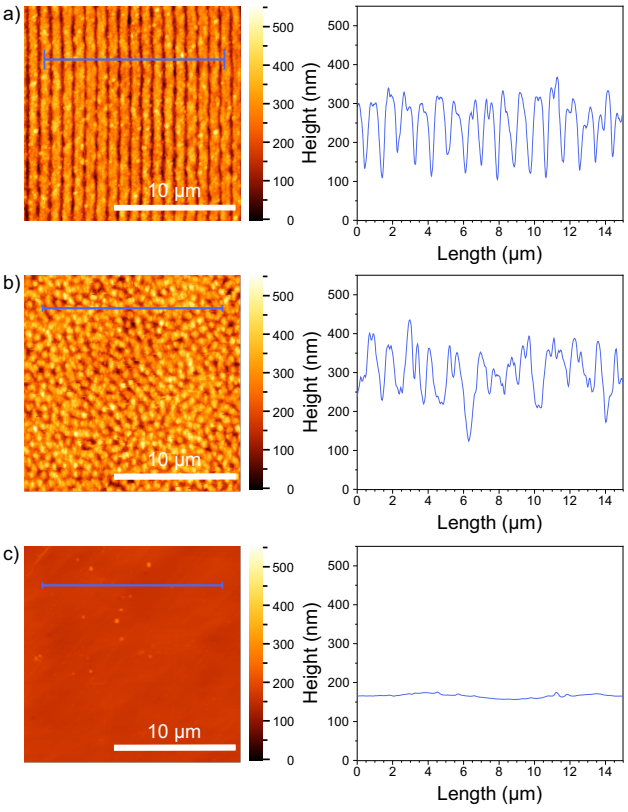

Fig. 2: Topography of the LIPSS fabricated on steel surface. AFM maps of (a) groove-like LIPSS, (b) spike-like LIPSS, and (c) the polished steel surface. The blue lines indicate the positions of the extracted height profiles.

The polished steel surface, which acts as a reference substrate for the performed cell culture experiments, is shown in Figure 2c. The RMS is 5 nm, and the maximum height difference observed in the shown profile is 18 nm. For moderate structure depths as fabricated here, the periodicity of LIPSS can be approximated based on the effective wavelength λ_{SPP} of the surface plasmons excited at the laser beam frequency on the steel-air interface. Using the surface plasmon dispersion relation, we obtain an effective wavelength of $\lambda_{\mathrm{SPP}} = 955$ nm. Here, a laser wavelength of 1030 nm, a dielectric constant of iron $\varepsilon_1 = -6.715 + i23.10$, and air as the surrounding medium was used [8]. The effective wavelength is very close to the observed LIPSS periodicity, confirming the ability to predict the structure geometry by the plasmon wavelength.

Next, the growth of EC was investigated on the three types of steel surfaces. The cells were segmented using Cellpose with the pre-trained neural network-based cyto3 model [6, 7]. Figure 3 shows a typical fluorescence image of the ECs on a polished surface and the corresponding image with the segmented cells color-marked. This segmentation is very robust and allows a fully automated cell analysis with respect to cell orientation and cell morphology.

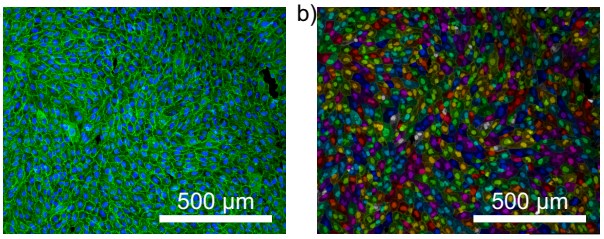

Fig. 3: Cell segmentation using the neural network based Cellpose model. (a) A fluorescence image of endothelial cells on a polished steel surface and (b) the same image with each detected cell color-coded.

Figure 4 shows a direct comparison of typical images of ECs on the groove-like LIPSS, the spike-like LIPSS, and the polished steel surface. The orientation of the groove-like LIPSS is along the direction indicated by an angle of 0° (cf. electron micrograph Figure 4a). The fluorescence images show no differ-

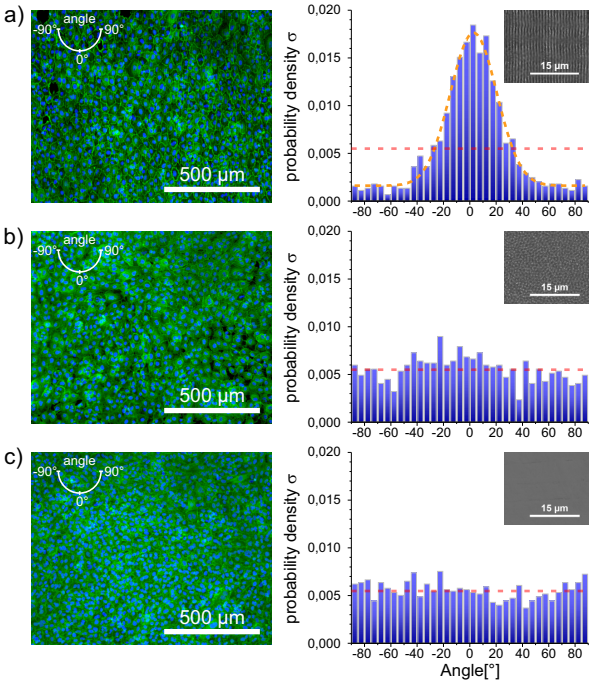

Fig. 4: Endothelial cells on the (a) groove-like LIPSS, (b) spike-like LIPSS, and (c) the polished surface. For each image, the probability density of the cell orientation is plotted. The ideal density for equally distributed orientation is indicated by the red dashed lines. The orange dashed line shows a Gaussian fit.

ences in the cell density for the three surfaces. However, when the probability density of the detected cells is analyzed with respect to the orientation angle, a distinct effect of the LIPSS becomes apparent. For the spike-like LIPSS and the polished surface, the cells are equally oriented at all angles. In stark contrast, the cells on the groove-like LIPSS show a preferred orientation along the grooves. The probability was fitted by a Gaussian, revealing a standard deviation of 18°. Thus, the fabricated groove-like LIPSS on the stainless steel allows a very controlled adjustment of the EC orientation. The median of the cell's aspect ratio varies between 1.47 and 1.67 and shows no dependency on the surface structure. Thus, the fabricated LIPSS have no distinct impact on the cell morphology.

Finally, we fabricated a stainless steel stent possessing LIPSS on its surface. The non-structured stent was mounted into the laser system and raster scanned by the laser beam. An electromicrograph of the stent is shown in Figure 5. The corresponding zoom-in image illustrates the quality of the groove-like LIPSS. The structure is very homogeneous over the entire outer stent surface without defects caused by inertia-induced movements or rotation mismatch. The groove orientation was

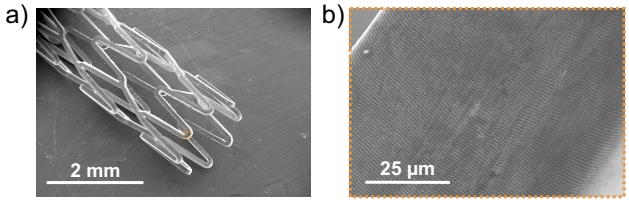

Fig. 5: LIPSS fabricated on a stainless steel stent. (a) Electron micrograph of the stent with the corresponding (b) zoom-in, showing the groove-like LIPSS.

chosen to be parallel to the stent's longitudinal axis and can be adjusted for the desired cell orientation by changing the polarization axis of the laser beam. However, the structure only covers the outer surface of the stent. A surface structure oriented towards the lumen would also be of great interest but would require some modifications to the laser system.

4 Conclusion

In conclusion, we investigated the use of groove-like and spike-like LIPSS on stainless steel surfaces to control endothelialization. First, an industrial femtosecond laser system was used to structure polished steel substrates (316L). The behavior of the ECs was analyzed by means of fluorescence imaging. The cells were segmented by a neural network-based model to analyze cell orientation and cell morphology. No distinct differences were found for spike-like LIPSS and the polished surface. However, on the groove-like LIPSS, the ECs show a preferred orientation parallel to the groove axis. The probability density of the cell's orientation shows a Gaussian distribution with a standard deviation of 18°. Finally, we fabricated LIPSS on an electro-polished stainless steel stent to demonstrate the use of LIPSS in industrial fabrication processes. The obtained surface structure was very homogeneous over the stent surface. For further adjustment of the endothelialization, the dimensions of the fabricated LIPSS and their orientation can be modified by process parameters like pulse energy and polarization direction. However, to implement LIPSS on the entire stent surface, modification of the laser system is inevitable. Nonetheless, LIPSS are a promising alternative to control endothelialization on commercial cardiovascular implant surfaces.

Author Statement

Financial support by the European Regional Development Fund (ERDF) and the European Social Fund (ESF) within the collaborative research between economy and science of the state Mecklenburg-Vorpommern is gratefully acknowledged.
Conflict of interest: Authors state no conflict of interest.

References

[1] Bekmurzayeva A, Duncanson WJ, Azevedo HS, Kanayeva D. Surface modification of stainless steel for biomedical applications: Revisiting a century-old material. Materials Science and Engineering: C. 2018; 93:1073–89.

[2] Mirhosseini N, Li L, Liu Z, Mamas M, Fraser D, Wang T. A comparison of endothelial cell growth on commercial coronary stents with and without laser surface texturing. Heliyon. 2024;10:e26425.

[3] Greiner A M, Sales A, Chen H, Biela S A, Kaufmann D, and Kemkemer R. Nano- and microstructured materials for in vitro studies of the physiology of vascular cells. Beilstein J. Nanotechnol. 2016; 7:1620–1641.

[4] Dong J, Pacella M, Liu Y, Zhao L. Surface engineering and the application of laser-based processes to stents - A review of the latest development. Bioactive Materials. 2022; 10:159–84.

[5] Nozaki K et al. Hierarchical periodic micro/nano-structures on nitinol and their influence on oriented endothelialization and anti-thrombosis. Mater. Sci. Eng. C 2015; 57:1-6.

[6] Stringer C, Wang T, Michaelos M, Pachitariu, M. Cellpose: a generalist algorithm for cellular segmentation. Nature methods 2021; 18:100-106.

[7] Stringer C, Pachitariu M. Cellpose3: one-click image restoration for improved cellular segmentation. Nature Methods 2025; 22:592-599.

[8] Johnson P B, Christy R W. Optical constants of transition metals: Ti, V, Cr, Mn, Fe, Co, Ni, and Pd. Phys. Rev. B 1974; 9:5056-5070.